Scientific Publishing House

Trends in Ecological and Indoor Environmental Engineering

Abdulhalim Musa Abubakar et al. *TEIEE 2(2) 2024*

RESEARCH ARTICLE **OPEN ACCESS**
https://doi.org/10.62622/TEIEE.024.2.2.11-23 **ISSN 2956-9761**

REVOLUTIONIZING BIODIESEL SYNTHESIS: KINETIC AND THERMODYNAMIC INSIGHTS WITH CARBONIZED DOUM-SHELL CATALYST

Abdulhalim Musa Abubakar[1], Haruna Mavakumba Kefas[1*], Yusufu Luka[1], Jimzibea Jehu Kawuwa[1]
[1]Department of Chemical Engineering, Faculty of Engineering, Modibbo Adama University, P.M.B. 2076, Yola, Adamawa State, Nigeria
*Corresponding email: hmkefas@mau.edu.ng

Received: 14.06.2024; ***Accepted:*** 29.06.2024; ***Available online:*** 30.06.2024 ***Published:*** 30.06.2024

Cite this article: Abubakar, A. M., Kefas, H. M., Luka, Y., & Kawuwa, J. J. (2024). Revolutionizing Biodiesel Synthesis: Kinetic and Thermodynamic Insights with Carbonized Doum-Shell Catalyst. *Trends in Ecological and Indoor Environment Engineering*, 2(2), 11–23.

Background: Conventional methods of biodiesel (FAME) synthesis often involve transesterification processes that are catalysed by homogeneous catalysts, which present challenges in terms of catalyst recovery, environmental impact, and production cost. Heterogeneous catalysts, particularly those derived from agricultural waste, have emerged as promising alternatives due to their reusability, environmental friendliness, and cost-effectiveness. **Objectives:** The study aims to bridge gaps by providing a comprehensive kinetic analysis of biodiesel production using a synthesized and novel, doum-shell catalyst. It incorporates first, second, and third-order rate model kinetics, alongside the determination of some energy parameters. **Methods:** Doum palm shell (DPS) was characterized by Fourier Transform Infrared (FTIR) and Atomic Force Microscope (AFM), and then carbonized, ground, and sulfonated to create a biochar catalyst, which was then used in the esterification of palmitic acid (PA) with methanol. Kinetic modelling of the esterification process was performed, followed by deriving thermodynamic parameters using Arrhenius and Eyring-Polanyi equations. **Results:** Kinetic modelling identified the First-Order reaction as the most appropriate for describing the esterification process at an optimum performing temperature of 55 °C, 180 min reaction time and rate constant, $k = 7 \cdot 10^{-4}$ min^{-1}. Thermodynamic parameters were derived from the Arrhenius and Eyring-Polanyi equations, providing a deeper understanding of the energy changes involved in the esterification reaction. The activation energy, pre-exponential factor, entropy, enthalpy and free energies obtained for the First-Order, describe the catalysing of the synthesis process by DPS as robust, reversible, non-spontaneous, feasible and energy efficient. In both kinetics and thermodynamics carried out, the Second- and Third-Order of reaction analysis described the experimental data poorly due to lower R^2 values comparative to the First-Order rate at 45, 55 and 65 °C. FTIR analysis confirmed the successful conversion of feedstock to biodiesel, with distinct ester functional groups such as, –OH, $–SO_3H$ and –COOH groups, identified in the DPS catalyst. **Conclusion:** This research lays the groundwork for future studies and large-scale implementation of this catalyst in biodiesel production, particularly in regions with abundant doum palm resources. Through comprehensive experimentation and analysis, the carbonized doum-shell catalyst was demonstrated to be a viable and efficient option for FAME synthesis from PA and methanol.

Keywords: doum palm shell; biodiesel production; esterification; palmitic acid; sulfonation.

INTRODUCTION

Biodiesel (FAME) production has garnered significant attention as a sustainable alternative to fossil fuels, driven by the necessity to reduce greenhouse gas emissions and dependence on non-renewable energy sources (Harsono, 2011). Conventional methods of biodiesel synthesis often involve transesterification processes that are catalysed by homogeneous catalysts, which present challenges in terms of catalyst recovery, environmental impact, and production cost. In recent years, heterogeneous catalysts, particularly those derived from agricultural waste, have emerged as promising alternatives due to their reusability, environmental friendliness, and cost-effectiveness (Gurunathan & Ravi, 2015; Khan et al., 2021). Despite these advancements, there remains a substantial research gap in optimizing the kinetic models and understanding the mechanistic pathways of biodiesel production using novel heterogeneous catalysts. Most studies have focused on single-order kinetic models (Haryanto et al., 2020; Hazrat et al., 2022), overlooking the potential insights that can be gained from evaluating first, second, and third-order kinetics simultaneously. Moreover, the activation energy and pre-exponential factors, which are crucial for designing efficient industrial processes, are often not comprehensively determined for several novel catalysts. Doum palm shell (DPS) have only been used as adsorbent to remove lead from water (Alkali et al., 2022) and in cement production as composite (Liman et al., 2020; Seth et al., 2018). The production of biodiesel using carbonized DPS catalyst represents an innovative approach to valorise agricultural waste while addressing the need for effective and sustainable catalytic processes. Given that the sub-Saharan African region including Northern Nigeria can boost of significant amount of doum palm (Inuwa et al., 2023; Ogbole & Ademoh, 2021), it is capable of serving as a hub for FAME production in the future. Previous work had demonstrated the feasibility of using diverse catalyst type in biodiesel production (Avhad & Marchetti, 2015; Bohlouli & Mahdavian, 2019); however, these studies have primarily concentrated on basic performance metrics without delving into detailed kinetic and thermodynamic analyses or the influence of reaction parameters.

This study aims to bridge these gaps by providing a comprehensive kinetic analysis of biodiesel production using a synthesized, carbonized doum-shell catalyst. The research incorporates first, second, and third-order rate model kinetics, alongside the determination of activation energy and pre-exponential factors. Furthermore, the study examines the esterification of palmitic acid (PA) as a free fatty acid (FFA) feedstock, employing advanced characterization techniques such as Fourier Transform Infrared (FTIR) and Atomic Force Microscope (AFM) to analyse the DPS catalyst. PA is a saturated fatty acid commonly found in both animal fats and vegetable oils. It is a major component of palm oil, typically comprising around 44 – 45% of the total fatty acids. PA is utilized in a variety of industrial applications, including the production of soaps, cosmetics, and food additives, due to its stabilizing properties and high melting point. Babajide (2011) defined FFA as fatty acids that are derived from phospholipids or triglycerides, when they are not attached to other molecules. Studies on PA-biodiesel production is not new (Carmo et al., 2009; Ghorbani-Choghamarani et al., 2022). In real-world scenarios, reactions may not strictly follow ideal kinetic models due to the presence of side reactions, catalyst deactivation, or

non-ideal mixing conditions. In the present work, the rate constants are determined, and the effects of temperature, reaction time, and conversion rates are systematically studied to determine the extent of the esterification reaction conformity with the ideal situations. Also, due to the fact that DPS catalyst is a novel catalyst that had not been previously reported in the literature, a thermodynamic study to determine the enthalpy, entropy and free energy requirements of the reaction, would complete the study. To implement that in the present study, insights from Noreen et al. (2021) will be applied.

MATERIALS AND METHODS

Doum Palm Shell carbonization

Doum palm fruits was locally obtained from the farm in Yola Metropolis, Adamawa State, Nigeria. About 500 g of DPS was cleaned, crushed, washed and spread on a sheet to sundry for 3 h, in order to remove its water content. After that, the DPS was carbonized in a furnace at a temperature of 250 ºC for 1.5 h under inert conditions. Then it was quenched with water before allowing it to cool at room temperature. The resultant biochar, shown in Figure 1a, was ground using mortar and pestle into fine powder. Figure 1b is a reflux batch system used by Callistus et al. (2016), in which the biochar sulfonation was carried out.

a

b

Figure 1. DPS biochar and a reflux batch system:
a – doum palm shell biochar; b – reflux batch system

Simply because the batch system, as concluded by Khan (2002), is a safe and convenient technique of obtaining kinetic data and screening catalyst.

Biochar sulfonation

Precisely 20 g of the doum palm biochar was sulphonated in a 3-necked round bottom flask using 200 mL of fuming H_2SO_4 at 130 ºC for 8 h under nitrogen flow. It was carried out by setting up a constant mixing process using a magnetic stirrer. After cooling to room temperature, the sulfonated DPS biochar was washed with distilled water, filtered with suction pump and oven-dried at 105 ºC for 15 h. About 20 g of the Doum palm shell (DPS) biochar was sulphonated in a 3-necked round bottom flask using 200 mL of fuming H_2SO_4. The purpose of washing with distilled water is to remove the excess acid. On the other hand, the drying of the washed sulfonated sample is to remove moisture. The dried sulfonated sample was subsequently characterized and used for the esterification reaction.

Catalyst characterization

Fourier Transform Infrared (FTIR) spectroscopy was used to qualitatively determine the functional group present in the structure of the catalyst. FTIR was conducted using a thermo-scientific PIKE Nicolet IS5 with built-in diamond surface using a screw-loaded anvil. Sample spectra were obtained using 32 scans for the wave number ranging from 650 – 4000 cm^{-1}. Secondly, AFM was used to generate a 3D scans, which measures the morphology, structure or compositional analysis of the samples. The 3D scans were conducted with an image size of 50 µm and a scan direction of up-time/line of 1 sec. They were performed using a cantilever type XYCONTR and a head type AFM, with a laser working point of 0.0% and a deflection offset of 0.0%. The scans were conducted in air, with a static force operating mode and a feedback mode of free-running. For this analysis, the software version used was 3.8.1.9 and the firmware version was 3.8.1.0. However, AFM is a powerful tool for imaging and characterizing surfaces at the nanoscale, and it can provide information about the topography, morphology, and other physical properties of a sample.

Free fatty acid determination

The FFA content of the oil was determined using official methods and recommended practices of the AOCS (Chang et al., 2016; Esan et al., 2024; İlgen, 2022). A precise quantity of crude palm oil was weighed into an Erlenmeyer flask and 75 mL of isopropanol, as well as 15 mL of n-hexane were added to the flask (Nandi et al., 2019). Following the specification in Chang et al. (2016), 3 drops of phenolphthalein solution were also added to the mixture and titrated against 0.1 N NaOH solution to a steady pink end-point, also obtained by Daniyan et al. (2019). The procedure was repeated twice and the average titre value of the NaOH used was recorded when the precision of each run does not exceed ±0.1, according to Mujeli et al. (2016). Thus, the FFA of the sample was calculated using Equation 1 (Japir et al., 2017).

$$\text{FFA value} = \frac{25.6 \cdot \text{Titre value} \cdot \text{Molarity}}{\text{Weight of Biodiesel}}. \quad (1)$$

In this work, 10 g of the PA feedstock was weighed. Afterwards, 12 g of methanol (CH_3OH) was also weighed using a weighing balance. The feedstock was poured into a round bottom flask followed by the CH_3OH. It was allowed to dissolve in the volume of CH_3OH. This process took 40 min to be achieved, then 3 g of the carbonized DPS catalyst was poured into the dissolved mixture. It consists of a thermometer and a magnetic stirrer placed in a round bottom flask, which was also placed in a pot of oil heated by a heating mantle. It is worthy of note that PA esterification with CH_3OH is a reversible process, but

the reverse reaction can be neglected based on making suitable assumptions (e.g., excess CH_3OH used), as mentioned by Hidayat et al. (2015) and Kostica et al. (2016). The heating was at 45, 55 and 65 ºC examined by Callistus et al. (2016) and for the duration of the biodiesel manufacture, which are 5, 30, 60, 90, 120, 150 and 180 min. After each reaction, the acid value of the esterified product and the FFA conversion yield were simultaneously calculated. The later was computed using Equation 2 (Ulfah et al., 2020).

$$\text{FFA Conversion } (\%) = \frac{AV_f - AV_p}{AV_f} \cdot 100, \quad (2)$$

where AV_f and AV_p are stands for the acid value of the feedstock and that of the product, respectively. The biodiesel produced using the optimum process conditions, was purified and analysed according to the European Committee for Standardization requirements.

Esterification kinetic analysis of FAME synthesis

Each sample was generated at 5, 30, 60, 90, 120, 150 and 180 min, at a specified temperature of 45, 55 and 65 ºC employed by Aisabor et al. (2016). It was then centrifuged to separate the biodiesel from the CH_3OH and the carbonized DPS. The FAME was taken and titrated individually. Using a measuring cylinder, 25 mL of ethanol was measured, and a gram of each of the biodiesel was taken and weighed on a weighing balance. The biodiesel was poured into a conical flask, followed by the ethanol and two drops of phenolphthalein. After that, titration was performed. Since the order of reaction is not known, an integral rate expression (Equations 3 – 5) based on an assumed order of reaction, n = 1, 2 and 3 was used (Brüning et al., 2015). Equation 3 is so because Jacob et al. (2008) mentioned that First-Order reactions depend on the concentration change of only one principal reactant and even when other reactants are present, each will assume an order of zero, and hence won't be present in the rate equation.

$$-\ln\left(\frac{C_{PA}}{C_{PA_0}}\right) = k_1 t, \quad (3)$$

$$\frac{1}{C_{PA}} = \frac{1}{C_{PA_0}} + k_2 t, \quad (4)$$

$$\frac{1}{C_{PA}^2} = \frac{1}{C_{PA_0}^2} + 2k_3 t, \quad (5)$$

where C_{PA_0} is initial FFA value or concentration of PA; C_{PA} is concentration of PA at time; t and k_n is rate constant.

Initially, valuable C_{PA}-time data were obtained at the specified temperatures and tabulated. Later, graphs were plotted in accordance to the response variable in Equations 3 – 5 and the respective k(s) was determined from the slope of the graph.

Thermodynamic study

The determined "k" values at a particular temperature were tabulated and Equation 6 was used to determine the unknown parameters (Chhabra et al., 2019; Moradi et al., 2015):

$$\ln k_n = \ln k_o - \frac{E_a}{R}\left(\frac{1}{T}\right), \quad (6)$$

where E_a is activation energy (kJ/mol); k_o is frequency factor, taking the universal gas constant; R = 8.314 kJ/(mol · K).

It was done by plotting $\ln k_n$ against $\frac{1}{T}$ (Sharma et al., 2020), where T is absolute temperature (K). A combination of Arrhenius and Eyring models (Equation 7) also details the dependence of k with the temperature. Based on Equation 8, a linear plot of $\ln\frac{k}{T}$ versus $\frac{1}{T}$ was carried out after taking the natural logarithm of Equation 7 (Suleiman et al., 2023). Then, using Equation 9 (Noreen et al., 2021), the Gibbs free energy change (ΔG) was determined.

$$k = k^* \cdot \frac{k_B T}{h} e^{-\frac{\Delta G}{RT}}, \quad (7)$$

$$\ln\frac{k}{T} = \frac{-\Delta H}{R}\left(\frac{1}{T}\right) + \left(\ln k^* + \ln\frac{k_B}{h} + \frac{\Delta S}{R}\right), \quad (8)$$

$$\Delta G = \Delta H - T\Delta S, \quad (9)$$

where k^* is transmission coefficient usually taken as 1; k_B = $1.38 \cdot 10^{-23}$ JK^{-1} is Boltzmann constant; ΔH is enthalpy change, kJ/mol; ΔS is entropy change, kJ/(mol · K); h = $6.63 \cdot 10^{-34}$ Js is Planck's constant.

RESULTS AND DISCUSSIONS

FTIR spectroscopy

FTIR spectroscopy measures the absorption of infrared radiation by the DPS catalyst sample. It is a graph of wavenumbers (cm^{-1}) on the x-axis and % transmittance on the y-axis. Figure 2a, which depicts the FTIR spectroscopy results of the DPS catalyst, indicates the presence of several functional groups that contribute to its efficacy as a precursor in biodiesel production.

The FTIR spectrum typically shows peaks corresponding to hydroxyl (–OH) groups, sulfonic acid (–SO_3H) groups, and possibly carboxyl (–COOH) groups. Hydroxyl groups presence is evidenced by broad absorption bands around 3200 – 3600 cm^{-1}, which are crucial for hydrophilicity and enhancing catalytic activity. Presence of sulfonic acid groups, with characteristic peaks around 1000 – 1300 cm^{-1}, significantly increases the acidic sites on the catalyst, which is essential for the esterification of FFAs into biodiesel. Additionally, carboxyl groups may appear as distinct peaks near 1700 cm^{-1}, further contributing to the catalyst's overall acidic nature. These functional groups collectively enhance the DPS catalyst's ability to efficiently catalyse the conversion of FFAs into biodiesel, making it a potent and viable bio-based catalyst for this purpose. According to Alkali et al. (2022), the presence of –OH and –COOH polar functional groups can also promote the adsorption of polar solute. With proper calibration, FTIR may also be used to analyse the FAME (Bradley, 2007), as well as the char displayed in Figure 2b.

In Figure 2b, the same functional group and peak ranges are shown for the char FTIR. Thus, the presence of these functional groups indicates that the char is also suitable for use as a catalyst in FAME production. While carboxyl groups are present, their impact might not be as significant as hydroxyl and sulfonic acid groups in the context of biodiesel production. This is due to the primary roles of –OH and – SO_3H groups in enhancing catalytic activity and increasing acidic sites, respectively. C-H stretching of alkanes is present around 2850 – 2950 cm^{-1}, but is not particularly impactful for the catalytic process in FAME production.

AFM analysis

Images obtained following an AFM analysis, were recorded at different magnification and particle sizes, as shown in Figure 3. It appears that Figure 3a and 3b are 3D scans of sample A and sample B, respectively, obtained using an AFM analyser.

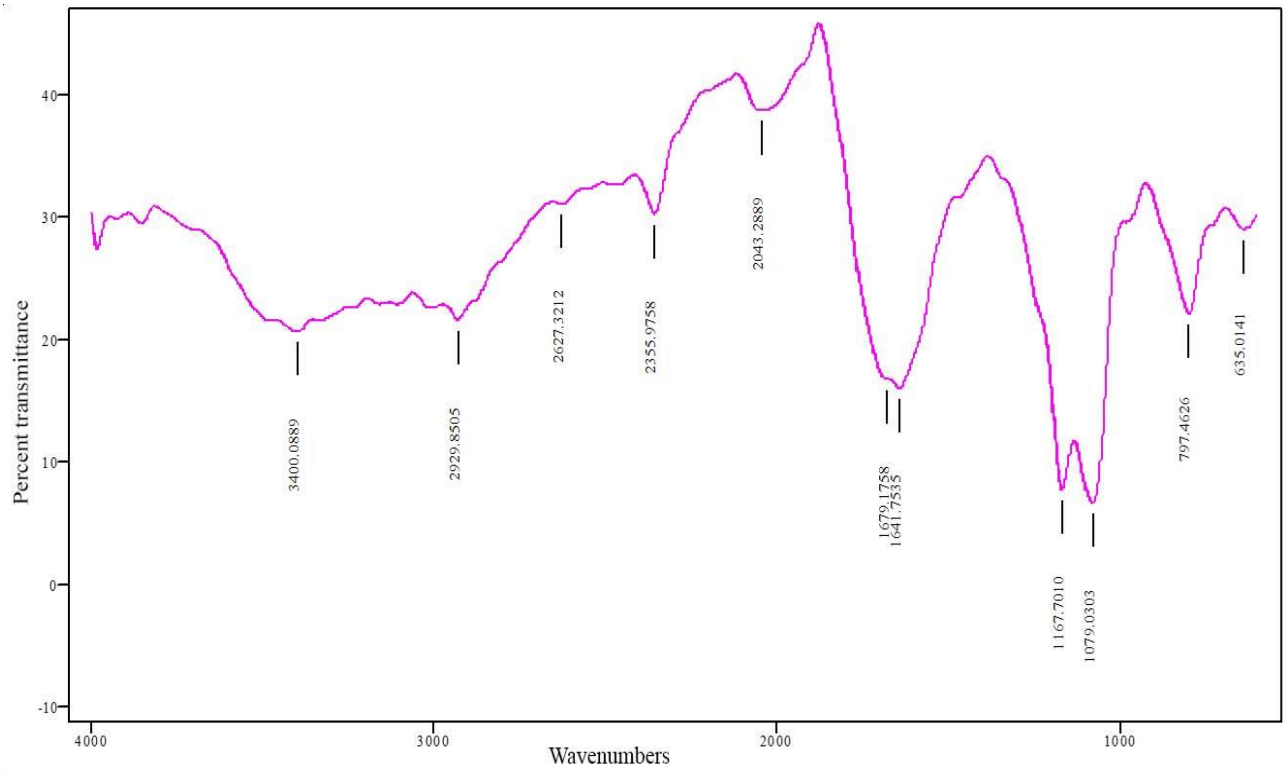

a

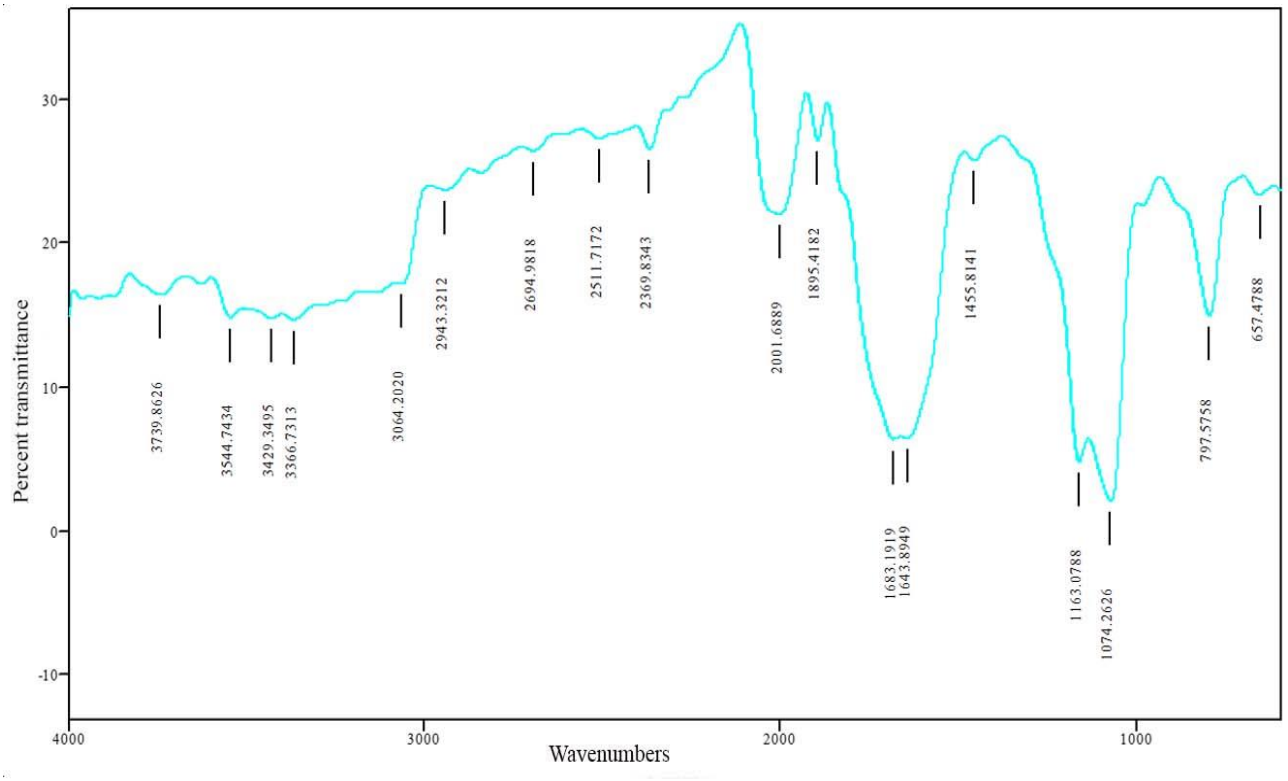

b

Figure 2. FTIR spectroscopy: a – FTIR spectroscopy of DPS catalyst; b – doum palm char FTIR spectroscopy

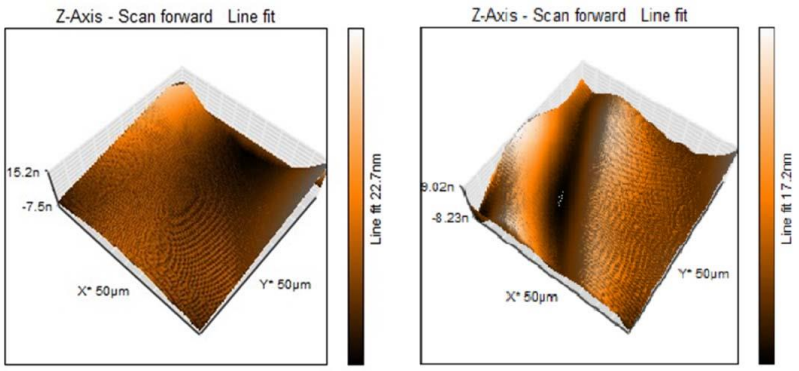

Figure 3. 3D scan group: a – sample A; b – sample B

Sample A and sample B, displayed in Figures 3a and 3b respectively, highlight the uniformity and texture of the sulfonated DPS biochar. These scans reveal a relatively smooth and consistent surface, with some variations in particle size and distribution. The fine texture and even surface morphology are indicative of effective sulfonation and carbonization processes, which are crucial for enhancing the catalytic activity. Such detailed topographical information provided by the AFM images aid the visualization of the surface characteristics that contribute to the high surface area and the availability of active sites for the esterification reaction. As a result, this comprehensive surface analysis confirms that the synthesized DPS catalyst possesses the desired structural properties, which are essential for its efficient performance in biodiesel production.

Effect of temperature and reaction time

Figures 4 and 5 respectively show the effect of reaction time on FFA concentration and % conversion at various temperatures. Figure 4 shows a decreasing trend in FFA concentration over time, as the FFAs are converted to FAME through the esterification reaction. In this study, adequate reaction time of 180 min which is also employed by Nandi et al. (2019), was allowed to favour the complete conversion of triglycerides into esters, as suggested by Eevera et al. (2009).

Obviously, the highest temperature of 65 °C increases the rate of the esterification reaction, leading to faster conversion of FFAs to FAME, as shown in Figure 5. However, excessively high temperatures can also lead to side reactions or degradation of the reactants, which can reduce the overall yield of FAME.

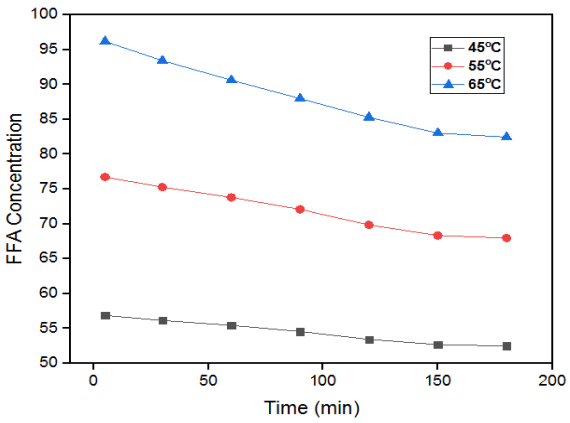

Figure 4. Concentration of FFA with time at different temperatures

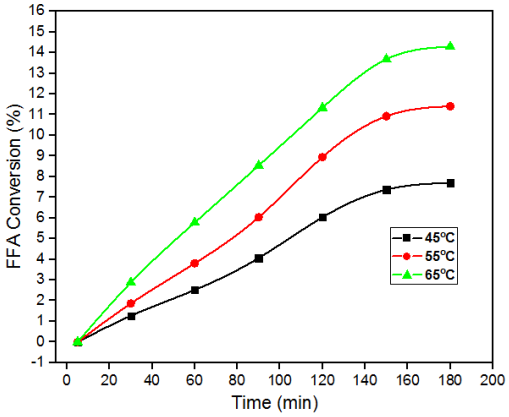

Figure 5. Percent FFA conversion with time for different temperature

Therefore, the most favourable temperature condition for the esterification reaction would depend on a balance between the rate of conversion (Table 1) and the overall yield of FAME. Nevertheless, the rising curve in Figure 5 is typical of X_{PA}-time plot described in the literature (Camara & Aranda, 2011), showing that the biodiesel yield increases with reaction time (Haryanto et al., 2020; Hazrat et al., 2022, 2023).

Table 1. Percent Conversion of PA

Time, min	X_{PA} , %		
	45 °C	55 °C	65 °C
5	0	0	0
30	1.266268	1.863921	2.879418
60	2.514949	3.806048	5.779626
90	4.06261	6.034932	8.534304
120	6.03236	8.941606	11.33056
150	7.368976	10.92284	13.67983
180	7.70313	11.40511	14.29314

As mentioned, the optimal temperature condition would likely be the one that provides the highest conversion rate with the highest overall yield of FAME (i.e., 14.29%). Because as the temperature increases, the rate of the esterification reaction becomes faster, leading to a higher rate of conversion of FFAs to FAME over time (Ceran et al., 2024). As time increases from 0 – 180 min, the conversion of FFAs to FAME surge at all temperatures, as more of the reactants are converted. There may be a point of diminishing returns, where further increase in time won't lead to any significant rise in conversion. Moreso, it was realized that the DPS catalyst maintained its activity and stability even after 5 cycles, in consonance with the findings of Amesho et al. (2022) – and indicating its potential for commercial applications. Arifin (2009) stated that a catalyst is normally recovered unaltered and doesn't

appear in the product, and further report that superfluous amount of catalyst would lead to reduced biodiesel yield and higher amount of synthesis cost. Rajalingam et al. (2020) also identified cost as one of the major factors to consider during biodiesel production.

First order kinetics

Dependent variable in the First-Order kinetic model is typically the natural logarithm of the ratio of the initial concentration of FFAs (C_{PA_0} = 56.86, 76.72 and 96.2 units) to the concentration of FFAs at a given time (C_{PA}), at the respective temperatures. The independent variable is typically the reaction time.

The slope of the line obtained from plotting the dependent variable against the independent variable in Table 2 represents the rate constant for the reaction.

Table 2. First order dependent and independent variable computations

Time, min	45 °C		55 °C		65 °C	
	Conc.	$-\ln\left(\frac{C_{PA}}{C_{PA_0}}\right)$	Conc.	$-\ln\left(\frac{C_{PA}}{C_{PA_0}}\right)$	Conc.	$-\ln\left(\frac{C_{PA}}{C_{PA_0}}\right)$
5	56.86	0	76.72	0	96.2	0
30	56.14	0.0127435	75.29	0.0188151	93.43	0.0292169
60	55.43	0.0254711	73.8	0.0388037	90.64	0.0595337
90	54.55	0.0414744	72.09	0.0622471	87.99	0.0892062
120	53.43	0.0622197	69.86	0.0936692	85.3	0.1202549
150	52.67	0.0765461	68.34	0.1156672	83.04	0.1471069
180	52.48	0.08016	67.97	0.121096	82.45	0.1542373

Figure 6 (depicting $C_{PA_0} \equiv C_{A_0}$ & $C_{PA} \equiv C_A$) represent the rate plots at 45, 55 and 65 °C for the First-Order model, whose trend is in agreement with plots at 50, 55 and 60 °C by Hazrat et al. (2022). These plots are used to assess the fit of the First-Order model at different temperatures. To determine which plot gives the best fit, it is essential to consider the coefficient of determination (R^2 values) for each plot. The R^2 value indicates how well the data fits the First-Order kinetic model. A higher R^2 value suggests a better fit of the model to the experimental data. Herein, the best occurred at 55 °C, as shown in Figure 6b. Because, at 45 °C, the reaction rate is relatively slow, indicating insufficient energy for optimal catalyst activity. At 55 °C, the reaction rate improves significantly, showing a steeper increase in esterified product concentration, which suggests this temperature is more favourable for efficient conversion of FFAs to biodiesel. At 65 °C, the reaction rate is the highest, but the potential for side reactions and reactant degradation increases.

This is not always the case as the optimal was 60 – 70 °C in Boonnoun et al. (2008). Thus, 55 °C is identified as the optimal temperature, balancing reaction efficiency and stability, ensuring effective conversion without the risks associated with higher temperatures.

As reiterated in the foregone, the deficiency of the worst performing temperature, in terms of fit, can be described by its lower R^2 value. Thus, at 65 °C the First-Order kinetic model moderately captures the behaviour of the esterification reaction. To correct the deficiency, reaction engineers must try to comprehend the underlying reaction mechanism and consider more complex kinetic models that account for intermediate species or complex reaction pathways to improve the model fit.

Second order kinetics

In Table 3, the computations are likely related to the Second-Order kinetic model, where the dependent and independent variables values differ based on the specific form of the temperature chosen for the second-order rate model analysed.

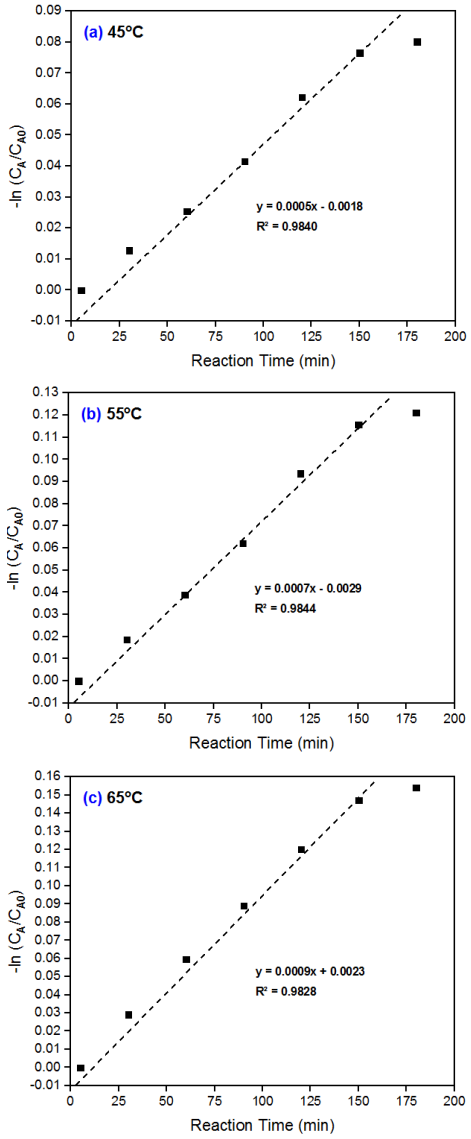

Figure 6. First order kinetics at 45, 55 and 65 °C

Table 3. Second order dependent and independent variable computations

Time, min	45 °C		55 °C		65 °C	
	Conc.	$\frac{1}{C_{PA}}$	Conc.	$\frac{1}{C_{PA}}$	Conc.	$\frac{1}{C_{PA}}$
5	56.86	0.017587	76.72	0.013034	96.2	0.010395
30	56.14	0.017813	75.29	0.013282	93.43	0.010703
60	55.43	0.018041	73.8	0.01355	90.64	0.011033
90	54.55	0.018332	72.09	0.013872	87.99	0.011365
120	53.43	0.018716	69.86	0.014314	85.3	0.011723
150	52.67	0.018986	68.34	0.014633	83.04	0.012042
180	52.48	0.019055	67.97	0.014712	82.45	0.012129

Due to differences in the models, "k" values would differ between the First-Order and second-order kinetic models. The rate constant in the First-Order model (k_1) represents the rate of the esterification reaction, while the rate constant in the Second-Order model (k_2) have a different interpretation. Model fit was hence assessed to identify potential sources of discrepancy between the model and experimental data shown in Tables 2 – 4, using the R^2 values estimated. Given that the fits for the Second-Order model are closer to 100% for all temperatures, several factors must be considered before choosing the best fit, shown in Figure 7.

At 45 °C (Figure 7a), the reaction rate is the slowest, with the plot showing a gradual slope. R^2 value of 0.9844 for this temperature is relatively lower, indicating a less precise fit to the Second-Order kinetic model and suggesting inefficient conversion of PA to biodiesel at this lower temperature. At 55 °C (Figure 7b), the reaction rate improves significantly, evidenced by a steeper slope on the plot. An R^2 value of 0.9849 is higher than at 45 °C, indicating a better fit to the kinetic model. This suggests that 55 °C provides a more optimal environment for the esterification process, balancing efficiency and reaction speed. Lastly, at 65 °C (Figure 7c), the reaction rate is the highest, with the plot showing the steepest slope. The R^2 value (0.9860) is also high, reflecting a good fit to the Second-Order kinetic model. However, despite the faster reaction rate, the higher temperature increases the risk of side reactions and thermal degradation of reactants, which can negatively impact the overall yield and efficiency. Considering both the reaction rates and the R^2 values, 55 °C emerges as the optimal temperature for the esterification reaction. It offers a balanced combination of high efficiency and stability, ensuring effective conversion of PA to biodiesel while minimizing adverse effects associated with higher temperature.

Third order kinetics

In Table 4 and at 65 °C, the initial concentration of the FFA is 96.2 units. The $\frac{1}{C_{PA}^2}$ values start at 0.000108 at 5 min and increase to 0.000147 at 180 min. Clearly, the change in $\frac{1}{C_{PA}^2}$ is more pronounced, demonstrating the fastest reaction rate among the three temperatures. However, it is crucial to consider potential side reactions or thermal degradation at higher temperature.

But at 45 °C, C_{PA_0} is 56.86 units, with $\frac{1}{C_{PA}^2}$ values increasing from 0.000309 at 5 min to 0.000363 at 180 min in. This gradual increase suggests a steady consumption of PA. On the other hand, 55 °C values show a more significant change compared to 45 °C, which is representative of a faster reaction rate and higher efficiency.

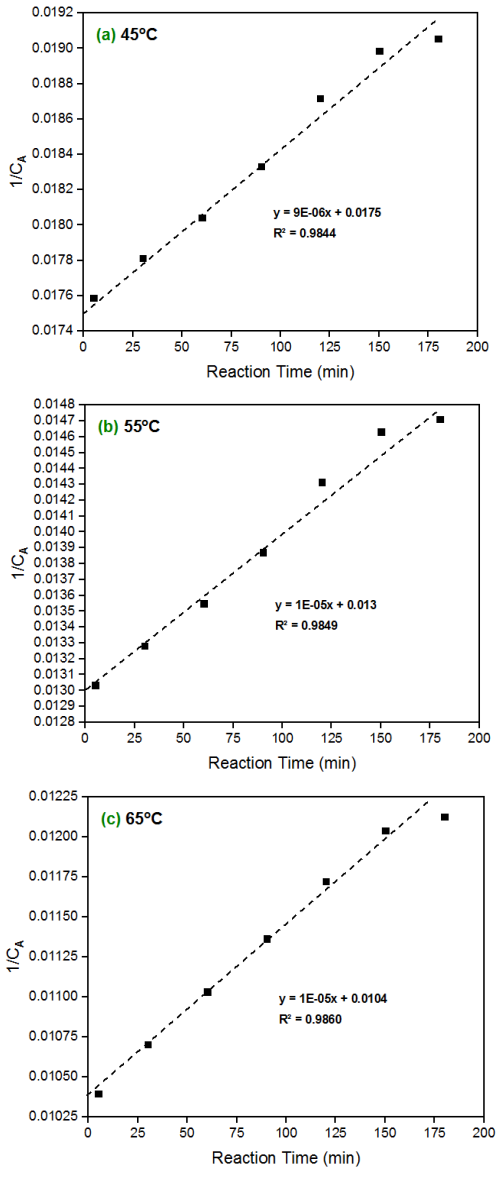

Figure 7. Second order kinetics plot for reaction temperatures at 45, 55 and 65 °C

R^2 values for the third-order kinetics plots in Figure 8 indicate varying degrees of fit across the temperatures. Given that the R^2 values for the third-order kinetic plots in Figure 8 show that 65 °C > 55 °C > 45 °C, this indicates that the data fits the third-order kinetic model best at 65 °C, followed by 55 °C, and least well at 45 °C.

Table 4. Third order dependent and independent variable computations

Time, min	45 °C		55 °C		65 °C	
	Conc.	$\frac{1}{C_{PA}{}^2}$	Conc.	$\frac{1}{C_{PA}{}^2}$	Conc.	$\frac{1}{C_{PA}{}^2}$
5	56.86	0.000309	76.72	0.00017	96.2	0.000108
30	56.14	0.000317	75.29	0.000176	93.43	0.000115
60	55.43	0.000325	73.8	0.000184	90.64	0.000122
90	54.55	0.000336	72.09	0.000192	87.99	0.000129
120	53.43	0.00035	69.86	0.000205	85.3	0.000137
150	52.67	0.00036	68.34	0.000214	83.04	0.000145
180	52.48	0.000363	67.97	0.000216	82.45	0.000147

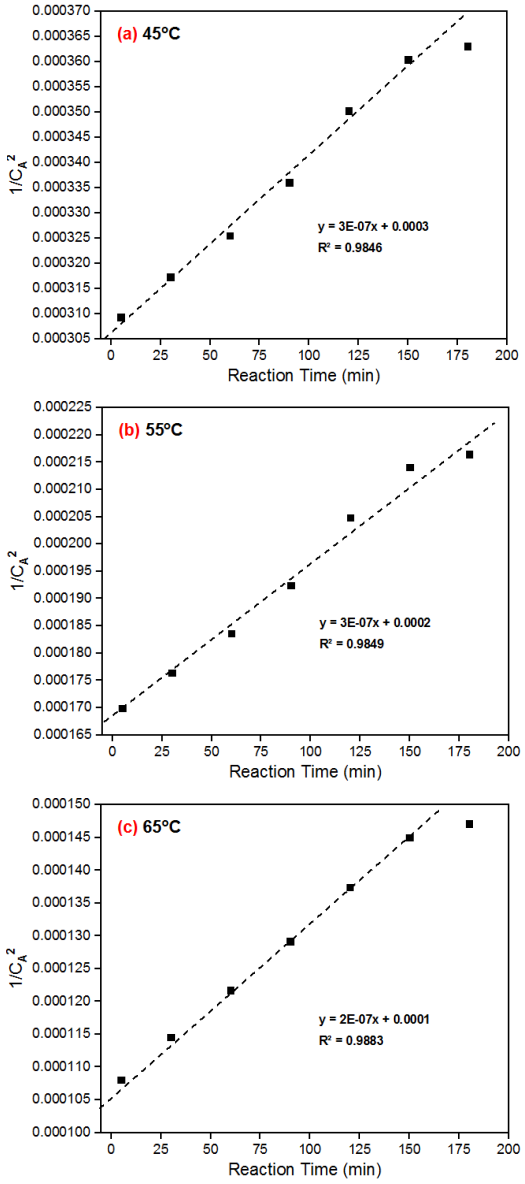

Figure 8. Third order kinetics at 45 °C, 55 °C and 65 °C

R^2 value at 55 °C, while slightly lower than at 65 °C, still indicates a good fit, suggesting that this temperature also supports the third-order reaction mechanism reasonably well. The fit at 45 °C is the poorest (Figure 8a), indicating that the lower temperature does not align as well with the third-order kinetic assumptions, possibly due to lower energy levels and slower reaction rates that deviate from the ideal model behaviour. Therefore, 65 °C is optimal for model accuracy, but 55 °C might be more practical for maintaining reaction stability and efficiency.

Calculated energy of activation

Table 5 represents the y- and x-axis variables computed to plot the activation energy graph in Figure 9, following the procedure showcased in Mahatale et al. (2019). In Table 5, k was observed to increase with temperature in agreement with Aisabor et al. (2016), but at n = 1 and n = 2. This phenomenon is in accordance with the Arrhenius equation, which describes the temperature dependence of reaction rates. This is due to the exponential term in the equation, which becomes larger with higher temperatures. As a result, the overall rate constant increases, indicating that the reaction proceeds at a faster rate at higher temperatures.

An increase in "k" with temperature (at n = 1 and n =2) can also be attributed to several factors. As the temperature rises, more molecules possess the necessary energy to overcome the activation energy barrier, leading to an increased frequency of successful collisions, and consequently a higher reaction rate. In another words, higher temperatures correspond to greater molecular kinetic energy, resulting in more frequent and energetic collisions between reactant molecules, which promotes the formation of product molecules. In this case k_1 and k_2 values at 65 °C, are greater than those at lower temperature, except for n = 3 where k_3 decreases to $1 \cdot 10^{-7}$ units. For the First-Order reaction (Figure 9a), the plot demonstrates a strong linear relationship with an R^2 value of 0.9958, just like in Javed et al. (2022) and Hazrat et al. (2023). This high R^2 value suggests that the First-Order kinetic model accurately represents the reaction mechanism, making it a suitable choice for describing the temperature dependence of the reaction rate. The calculated E_a for this order is 26.3055 kJ/mol.

In contrast, the second-order reaction (Figure 9b) shows a lower R^2 value of 0.7660, indicating a poorer fit to the experimental data compared to the First-Order model. This lower R^2 suggests that the second-order kinetic model does not capture the reaction dynamics as effectively. Using R = 8.314 kJ/(mol · K), and where the slope of Figure 9b is -0.5723, the activation energy is simply $E_a = 0.5723 \cdot 8.314 = 4.758102$ kJ/mol, which is significantly lower. The third-order reaction plot (Figure 9c) has the lowest R^2 value of 0.7337, indicating the weakest fit among the three models. This suggests that the third-order kinetic model is the least appropriate for describing the reaction's temperature dependence.

Table 5. Kinetic data for Arrhenius parameters determination

T, °C	T, K	$\frac{1}{T}$, K^{-1}	$\frac{1}{T} \cdot 10^{-3}$, K^{-1}	k_1	$\ln k_1$	$\ln \frac{k_1}{T}$
n = 1						
45	318	0.003145	3.145	0.0005	-7.6009	-13.363
55	328	0.003049	3.049	0.0007	-7.26443	-13.0574
65	338	0.002959	2.959	0.0009	-7.01312	-12.8362
n = 2						
45	318	0.003145	3.145	$9 \cdot 10^{-6}$	-11.6183	-17.3803
55	328	0.003049	3.049	$1 \cdot 10^{-5}$	-11.5129	-17.3059
65	338	0.002959	2.959	$1 \cdot 10^{-5}$	-11.5129	-17.336
n = 3						
45	318	0.003145	3.145	$1.5 \cdot 10^{-7}$	-15.7126	-21.4747
55	328	0.003049	3.049	$1.5 \cdot 10^{-7}$	-15.7126	-21.5056
65	338	0.002959	2.959	$1 \cdot 10^{-7}$	-16.1181	-21.9411

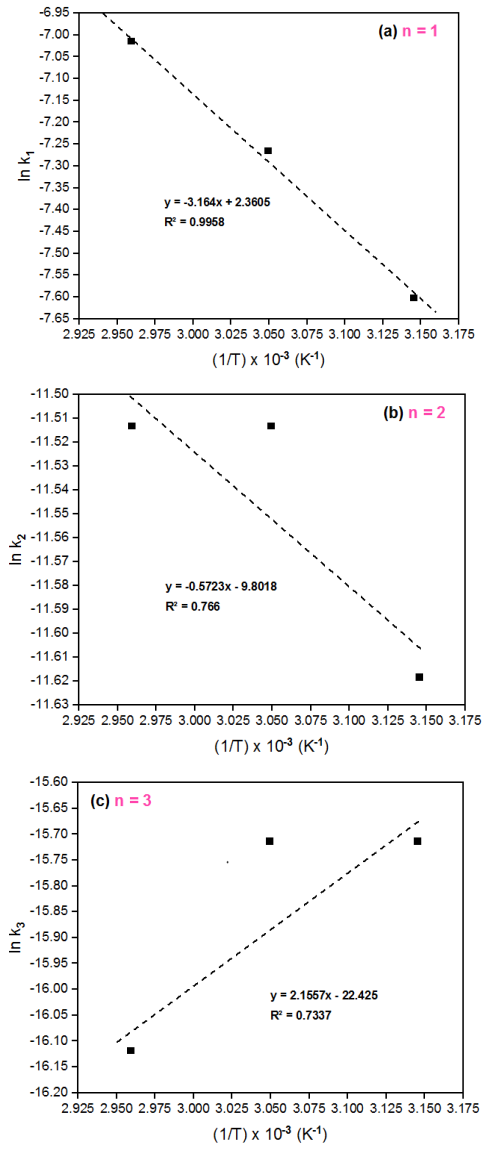

Figure 9. Arrhenius plot based on assumed reaction order

It is observed that E_a for the third-order reaction is negative, at -17.9225 kJ/mol (Table 6), which is physically implausible and further suggests that this model does not accurately describe the reaction mechanism. Javed et al. (2022) reported an E_a value ranging from 10 – 88 kJ/mol for several precursors in their research, which only brackets the E_a obtained at n = 1 in this study; as well as 55.08 kJ/mol reported by Kefas et al. (2020), in a similar study using palm fatty acid distillate (PFA). In close agreement with the present study (n = 1 in Table 6), Emeji et al. (2015) obtained an E_a = 23.44 kJ/mol when hexane was used as co-solvent.

Table 6. Activation energy and pre-exponential factors

Order	Parameter	Value
n = 1	E_a, kJ/mol	26.3055
	k_0, min^{-1}	10.59624
	R^2	0.9958
n = 2	E_a, kJ/mol	4.758102
	k_0, L/(mol · min)	$5.535 \cdot 10^{-5}$
	R^2	0.7660
n = 3	E_a, kJ/mol	-17.92249
	k_0, $L^2/(mol^2 \cdot min)$	$1.834 \cdot 10^{-10}$
	R^2	0.7337

Based on the data provided, the pre-exponential factors k_0 for reaction orders n =1, n = 2 and n = 3 are 10.59624 min^{-1}, $5.535 \cdot 10^{-5}$ L/(mol · min) and $1.834 \cdot 10^{-10}$ $L^2/(mol^2 \cdot min)$, respectively. These values decrease as the reaction order increases, indicating a lower frequency of effective collisions in higher-order reactions. The n = 1 model exhibits the highest efficiency with the highest k_0 and a very high R^2 value of 0.9958, suggesting it provides the best fit to the experimental data. In contrast, the n = 2 and n = 3 models have lower k_0 values and lower R^2 values (0.7660 and 0.7337, respectively), indicating potentially slower reaction rates and less accurate representation of the data compared to the n = 1 model. Therefore, for describing the kinetics observed in the data set, the n = 1 model stands out as the most efficient and accurate choice.

Enthalpy, entropy and Gibbs free energy

The aforementioned thermodynamic parameters were determined using Equations 7 – 9 utilizing the axis values in Table 5. From Figure 10, ΔH and ΔS was determined from the slopes and intercept of the straight-line equation (or linearized Equation 8), respectively.

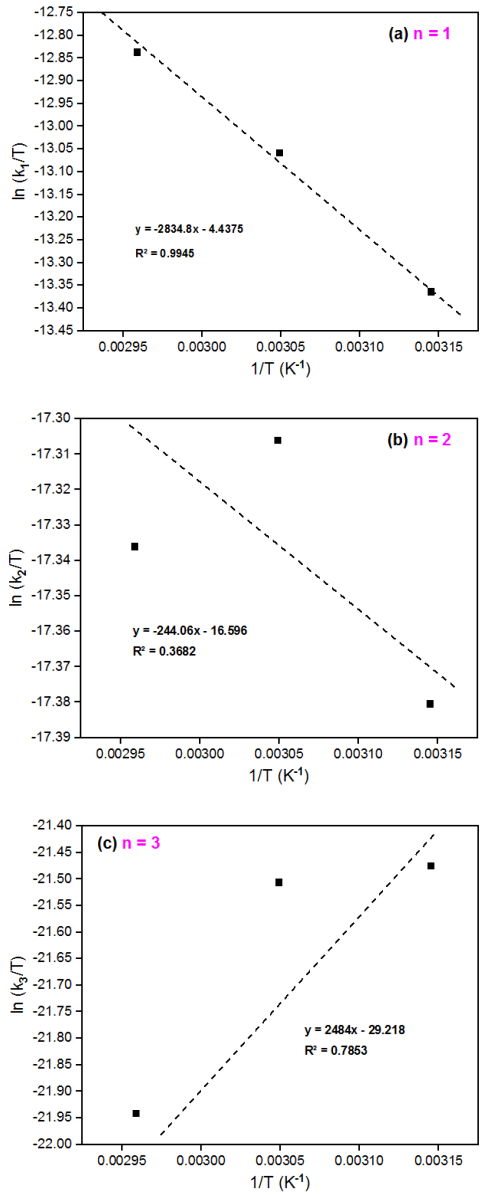

Figure 10. Graphical determination of enthalpy and entropy energies

By substituting all constant values in the intercept part of Equation 8, ΔH and ΔS can be computed using Equations 10 and 11.

$$\Delta H = -(8.314 \cdot \text{Slope}), \quad (10)$$

$$\Delta S = R(\text{Intercept} - 23.76). \quad (11)$$

As shown in Table 7, ΔH and ΔS for n = 1 and n = 2 have the same sign, but ΔH is negative for n = 3, implying a somewhat closer agreement when the order of reaction is 1 and 2. The positive ΔH at n = 1 and n = 2 imply an endothermic process while the negative ΔH at n = 3 implied an exothermic reaction. On the other hand, ΔS negativity points to an associative mechanism that is reversible (Noreen et al., 2021). In comparison with the fit in Figure 10, the First-Order energy terms in Table 7 seemed to align best with the empirical data. Only 36.8% goodness of fit was obtained at n = 2, which is significantly low. Even though the R^2 at n = 3 is higher than this value, it totally deviates from the true assumption.

Table 7. Energy change computed under different order of reaction

Order	Parameter	Value
n = 1	ΔH, kJ/mol	23568.53
	ΔS, kJ/(mol · K)	-234.434
	ΔG at 318K, kJ/mol	98118.54
	ΔG at 328K, kJ/mol	100462.9
	ΔG at 338K, kJ/mol	102807.224
	R^2	0.9945
n = 2	ΔH, kJ/mol	2029.115
	ΔS, kJ/(mol · K)	-335.52
	ΔG at 318K, kJ/mol	108724.4
	ΔG at 328K, kJ/mol	112079.6
	ΔG at 338K, kJ/mol	115434.802
	R^2	0.3682
n = 3	ΔH, kJ/mol	-20651.98
	ΔS, kJ/(mol · K)	-440.459
	ΔG at 318K, kJ/mol	119414
	ΔG at 328K, kJ/mol	123818.6
	ΔG at 338K, kJ/mol	128223.197
	R^2	0.7853

Thus, the First-Order model best describe the esterification of PA with CH_3OH to FAME. But then, ΔG is calculated for 45 °C (318K), 55 °C (328K) and 65 °C (338K) from Equation 9 and their relationship at the specified order of reaction is illustrated via Figure 11. In agreement with Suleiman et al. (2023), the fact that ΔG "s" is positive, makes the synthesis of biodiesel from DPS catalyst a non-spontaneous process.

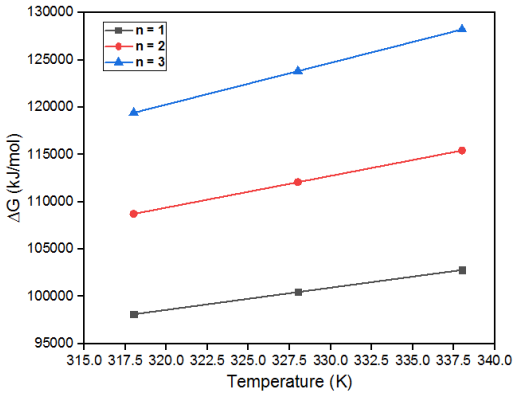

Figure 11. Effect of temperature variation with enthalpy change

It is observed that ΔG values for n = 1 are significantly lower than those for higher orders, as evidenced in Figure 11, which might suggest more realistic and feasible reaction parameters.

CONCLUSION

This research has advanced the understanding of the kinetics and thermodynamics involved in biodiesel production using an innovative carbonized doum-shell catalyst. The research demonstrated the potential of DPS as a sustainable and efficient catalyst for biodiesel synthesis, addressing both environmental and economic concerns associated with conventional catalysts. First-Order kinetic model was determined to be the most appropriate for describing the esterification process, with ΔH of 23,568.53 kJ/mol, ΔS of -234.434 kJ/(mol · K), and ΔG of 98,118.54 kJ/mol at 45 °C, 100,462.9 kJ/mol at 55 °C, and 102,807.224 kJ/mol at 65 °C. The best temperature for the

reaction was identified at 328 K, corresponding to an E_a of 26.31 kJ/mol and $k_0 = 10.596$ min^{-1}, which then points to a non-spontaneous and endothermic reaction. These values were corroborated by a high R^2 value of 0.9844, 0.9958 and 0.9945 from n = 1 rate model, Arrhenius equation and Eyring-Polanyi model, respectively, suggesting the reliability and accuracy of the model. FTIR analysis confirmed the successful conversion of feedstock to biodiesel, showing characteristic peaks that correspond to ester functional groups. The findings advocate for the scalability of this approach, potentially transforming biodiesel production in regions abundant with doum palm resources, thereby promoting sustainable energy solutions. Limitations leading to deviations from the second and third order rate models should be studied and addressed.

Author's statements

Acknowledgements

We thank our respected reviewers for their valuable comments and suggestions that helped us to improve this paper.

Contributions

All authors contributed to the study's conception and design. Conceptualization: H.M.K.; Data curation: Y.L., H.M.K.; Formal analysis: A.M.A., J.J.K.; Investigation: H.M.K., J.J.K., Y.L.; Methodology: J.J.K., Y.L.; Project administration: H.M.K., Y.L.; Software: A.M.A.; Supervision: H.M.K., A.M.A.; Validation: A.M.A., H.M.K.; Visualization: A.M.A., H.M.K.; Writing – original draft: A.M.A., H.M.K..; Writing – review & editing: H.M.K.

Declaration of conflicting interest

The authors declare no competing interests.

Financial interests

The authors declare they have no financial interests.

Funding

Not applicable.

Data availability statement

No data were used for the current study.

AI Disclosure

The author declares that generative AI was not used to assist in writing this manuscript.

Ethical approval declarations

Not applicable.

Additional information

Publisher's note

Publisher remains neutral with regard to jurisdictional claims in published maps and institutional affiliations.

REFERENCES

Aisabor, W., Lukman, Y., Otaru, A. J., Anakhu, A. E., & Otoikhian, S. K. (2016). Optimisation and kinetics of rubber seed oil biodiesel production. *Journal of Biofuels*, 7(2), 53–61. https://doi.org/10.5958/0976-4763.2016.00008.8.

Alkali, M. I., Abdus-Salam, N., Dikwa, M. K., Oyewumi-Musa, R. T., Jimoh, A. A., Ojo, I., & John, G. (2022). Adsorption of Pb (II) ion onto modified doum palm (Hyphaene thebaica) shells: Isotherm, kinetic and thermodynamic studies. *Arid Zone Journal of Basic and Applied Research (AJBAR)*, 1(5), 80–102. https://doi.org/10.55639/607gfedc.

Amesho, K. T. T., Lin, Y.-C., Chen, C.-E., Cheng, P.-C., & Ponnusamy, V. K. (2022). Optimization and kinetics studies of biodiesel synthesis from Jatropha curcas oil under the application of eco-friendly microwave heating technique: An environmentally benign and sustainable bio-waste management approach. *Sustainable Environment Research*, 32(41), 1–13. https://doi.org/10.1186/s42834-022-00151-w.

Arifin, S. F. (2009). *Production of biodiesel from waste cooking oil and RBD palm oil using batch transesterification process* (R. Abdul Rasid (ed.)) [Degree of Bachelor of Chemical Engineering, Faculty of Chemical & Natural Resources Engineering, Universiti Malaysia Pahang]. https://core.ac.uk/download/pdf/159177474.pdf.

Avhad, M. R., & Marchetti, J. M. (2015). A review on recent advancement in catalytic materials for biodiesel production. *Renewable and Sustainable Energy Reviews*, 50, 696–718. https://doi.org/10.1016/j.rser.2015.05.038.

Babajide, O. O. (2011). *Optimisation of biodiesel production via different catalytic and process systems* (L. Petrik, F. Ameer, & B. Amigun (eds.)) [MSc (Industrial Chemistry) Philosophiae Doctor in the Department of Chemistry, University of the Western Cape]. https://core.ac.uk/download/pdf/58914181.pdf.

Bohlouli, A., & Mahdavian, L. (2019). Catalysts used in biodiesel production: A review. *Biofuels*, 1–14. https://doi.org/10.1080/17597269.2018.1558836.

Boonnoun, P., Maneesiri, A., & Pattamaprom, C. (2008). Production of biodiesel from palm fatty acid distillate. *Thammasat International Journal of Science and Technology*, 13(4), 32–37. https://doi.org/https://ph02.tci-thaijo.org/index.php/SciTechAsia/article/view/41418.

Bradley, M. (2007). Biodiesel (FAME) analysis by FT-IR. *Thermo Scientific-Application Note, 51258*, 2–4. https://tools.thermofisher.com/content/sfs/brochures/AN-51258.

Brüning, M., Aylwin, C., & Alvarado, F. A. D. (2015). Differential equations on the kinetics of biodiesel production. *Fuel*, 142(303), 303. https://doi.org/10.1016/j.fuel.2014.09.117.

Callistus, U. N., Ndidi, A. F., Okechukwu, O. D., & Patrick, A. E. (2016). Reaction kinetics of biodiesel production from refined cottonseed oil using calcium oxide. *World Academy of Science, Engineering and Technology International Journal of Chemical and Molecular Engineering*, 10(6), 739–742. http://scholar.waset.org/1307-6892/10004677.

Camara, L. D. T., & Aranda, D. A. G. (2011). Reaction kinetic study of biodiesel production from fatty acids esterification with ethanol. *Industrial & Engineering Chemistry Research*, 50, 2544–2547. https://doi.org/10.1021/ie1005806.

Carmo, A. C., De Souza, L. K. C., Da Costa, C. E. F., Longo, E., Zamian, J. R., & Da Rocha Filho, G. N. (2009). Production of biodiesel by esterification of palmitic acid over mesoporous aluminosilicate Al-MCM-41. *Fuel*, 88(3), 461–468. https://doi.org/10.1016/j.fuel.2008.10.007.

Ceran, Z. D., Demir, V., & Akgün, M. (2024). Optimization and kinetic study of biodiesel production from Jatropha curcas oil in supercritical methanol environment using ZnO/γ-Al2O3 catalyst. *Biomass Conversion and Biorefinery*, 1–12. https://doi.org/10.1007/s13399-024-05307-9.

Chang, A. S., Sherazi, S. T. H., Kandhro, A. A., Mahesar, S. A., Chang, F., Shah, S. N., Laghari, Z. H., & Panhwar, T. (2016). Characterization of palm fatty acid distillate of different oil processing industries of Pakistan. *Journal of Oleo Science (JOS)*, 65(11), 897–901. https://doi.org/10.5650/jos.ess16073.

Chhabra, P., Mosbach, S., Karimi, I. A., & Kraft, M. (2019). Practically useful models for kinetics of biodiesel production [Research-article]. *ACS Sustainable Chemistry & Engineering*, 7, 4983–4992. https://doi.org/10.1021/acssuschemeng.8b05636.

Crymble, S. D. (2010). *Optimization and reaction kinetics of the production of biodiesel from castor oil via sodium methoxide-catalyzed methanolysis* (R. Hernandez & M. Zappi (eds.)) [Degree of Master of Science Graduate Thesis in Chemical Engineering, Dave C. Swalm School of Chemical Engineering, Mississippi State University]. https://scholarsjunction.msstate.edu/td/3395.

Daniyan, I. A., Bello, E. I., Ogedengbe, T. I., & Mogaji, P. B. (2019). Gas chromatography and Fourier Transform Infrared analysis of biodiesel from used and unused palm olein oil. *International Journal of Engineering Research in Africa*, 42, 47–64. https://doi.org/10.4028/www.scientific.net/JERA.42.47.

Eevera, T., Kaliaperumal, R., & Saradha, S. (2009). Biodiesel production process optimization and characterization to assess the suitability of product for varied environmental conditions. *Renewable Energy*, 34(3), 762–765. https://doi.org/10.1016/j.renene.2008.04.006.

Emeji, I. C., Afolabi, A. S., Abdulkareem, A. S., & Kalala, J. (2015). Characterization and kinetics of biofuel produced from waste cooking oil. *Proceedings of the World Congress on Engineering and Computer Science 2015 Vol II [WCECS 2015], October 21-23, 2015, San Francisco, USA, II*, 21–24.

Esan, A. O., Babalola, B. A., Raji, Y. A., Oladigbolu, M. A., Ajao, G. Q., Olawoore, I. T., & Adeyemi, A. D. (2024). Characterization of palm fatty acid distillate and soybean deodorized distillate for biodiesel production. *Journal of Applied Science and Environmental Management (JASEM)*, 28(5), 1461–1466. https://doi.org/10.4314/jasem.v28i5.17.

Ghorbani-Choghamarani, A., Taherinia, Z., & Tyula, Y. A. (2022). Efficient biodiesel production from oleic and palmitic acid using a novel molybdenum metal–organic framework as efficient and reusable catalyst. *Scientific Reports*, 12(10338), 1–12. https://doi.org/10.1038/s41598-022-14341-4.

Gurunathan, B., & Ravi, A. (2015). Process optimization and kinetics of biodiesel production from neem oil using copper doped zinc oxide heterogeneous nanocatalyst. *Bioresource Technology*, 190, 424–428. https://doi.org/10.1016/j.biortech.2015.04.101.

Harsono, S. S. (2011). Biodiesel production from palm oil technology. *Research Journal of Agricultural Science*, 43(4), 80–85. https://rjas.ro/download/paper_version.paper_file.8c1d65dd0a7154ef.313332352e706466.pdf.

Haryanto, A., Gita, A. C., Wahyusaputra, T., & Telaumbanua, M. (2020). First order kinetics of biodiesel synthesis using used frying oil through transesterification reaction. *Aceh International Journal of Science and Technology*, 9(1), 1–11. https://doi.org/10.13170/aijst.9.1.13297.

Hazrat, M. A., Rasul, M. G., Khan, M. M. K., Ashwath, N., Fattah, I. M. R., Ong, H. C., & Mahlia, T. M. I. (2023). Biodiesel production from transesterification of Australian Brassica napus L. oil: Optimisation and reaction kinetic model development. *Environment, Development and Sustainability*, 25, 12247–12272. https://doi.org/10.1007/s10668-022-02506-0.

Hazrat, M. A., Rasul, M. G., Khan, M. M. K., Ashwath, N., Silitonga, A. S., Fattah, I. M. R., & Mahlia, T. M. I. (2022). Kinetic modelling of esterification and transesterification processes for biodiesel production utilising waste-based resource. *Catalysts*, 12(1472), 1–37. https://doi.org/10.3390/catal12111472.

Hidayat, A., Rochmadi, Wijaya, K., Nurdiawati, A., Kurniawan, W., Hinode, H., Yoshikawa, K., & Budiman, A. (2015). Esterification of palm fatty acid distillate with high amount of free fatty acids using coconut shell char based catalyst. *Energy Procedia*, 75, 969–974. https://doi.org/10.1016/j.egypro.2015.07.301.

İlgen, O. (2022). Study on kinetics and reaction parameters of biodiesel production from sunflower oil and methanol using zinc oxide supported calcium oxide. *Periodica Polytechnica Chemical Engineering*, 66(2), 261–268. https://doi.org/10.3311/PPch.19198.

Inuwa, S. Z., Ndife, J., & Bamalli, Z. (2023). Review on functional values of doum palm fruit. *Dutse Journal of Pure and Applied Sciences (DUJOPAS)*, 9(3a), 29–40. https://doi.org/10.4314/dujopas.v9i3a.4.

Jacob, I., Clausen, E., & Carrier, D. J. (2008). *Kinetics determination of soybean oil transesterification in the design of a continuous biodiesel production process* [Biological and Agricultural Engineering Undergraduate Honirs Theses, University of Arkansas, Fayetteville]. https://scholarworks.uark.edu/baeguht/34.

Japir, A. A., Salimon, J., Derawi, D., Bahadi, M., Al-Shuja, S., & Yusop, M. R. (2017). Physicochemical characteristics of high free fatty acid crude palm oil. *Oilseeds & Fats Crops and Lipids (OCL)*, 24(5), 1–9. https://doi.org/10.1051/ocl/2017033.

Javed, F., Saif-ul-Allah, M. W., Ahmed, F., Rashid, N., Hussain, A., Zimmerman, W. B., & Rehman, F. (2022). Kinetics of biodiesel production from microalgae using microbubble interfacial technology. *Bioengineering*, 9(739), 1–17. https://doi.org/10.3390/ bioengineering9120739.

Jumaah, A. M., Yusoff, Mohamad Firdaus, M., & Salimon, J. (2018). Physicochemical properties and analysis of Malaysian palm fatty acid distilled. *The 2017 UKM FST Postgraduate Colloquium: AIP Conference Proceedings*, 1940(020092), 1–6. https://doi.org/10.1063/1.5028007.

Jumaah, M. A., Yusoff, M. F. M., Salimon, J., & Bahadi, M. (2019). Physical characteristics of palm fatty acid distillate. *Journal of Chemical and Pharmaceutical Sciences (JCPS)*, 12(1), 1–5. https://www.jchps.com.

Kefas, H. M., Yunus, R., Rashid, U., & Taufiq-yap, Y. H. (2020). Modified sulfonated glucose-catalyzed esterification of palm fatty acid distillate: Kinetics and fuel properties. *American Journal of Chemical Engineering (AJCE)*, 8(6), 131–138. https://doi.org/10.11648/j.ajche.20200806.12.

Khan, A. K. (2002). *Research into biodiesel kinetics & catalyst development* (V. Rudolph, Y. He, A. Hanley, & G. Kerven (eds.)) [Individual Inquiry A Thesis, Department of Chemical Engineering, The University of Queensland]. https://angelfire.com/ks3/go-diesel/files042803/adam_khan_thesis.pdf.

Khan, H. M., Iqbal, T., Yasin, S., Ali, C. H., Abbas, M. M., Jamil, M. A., Hussain, A., Soudagar, M. E. M., & Rahman, M. M. (2021). Application of agricultural waste as heterogeneous catalysts for biodiesel production. *Catalysts*, 11(1215), 1–19. https://doi.org/10.3390/catal11101215.

Kostic, M. D., Velickovic, A. V, Jokovic, N. M., Stamenkovic, O. S., & Veljkovic, V. B. (2016). Optimization and kinetic modeling of esterification of the oil obtained from waste plum stones as a pretreatment step in biodiesel production. *Waste Management*, 48, 619–629. https://doi.org/10.1016/j.wasman.2015.11.052.

Liman, A. Z., Adagba, T., & Umar, H. A. (2020). Effect of crushed doum palm shell as partial replacement of coarse aggregate in concrete. *FUDMA Journal of Sciences (FJS)*, 4(4), 1–9. https://doi.org/10.33003/fjs-2020-0404-45.

Mahatale, M., Kapoor, S., & Patil, D. (2019). Kinetics and thermodynamic studies of biodiesel production from used sun flower oil. *International Journal of Current Engineering and Scientific Research (IJCESR)*, 6(1), 624–633. https://troindia.in/journal/ijcesr/vol6iss1part3/624-633.pdf.

Moradi, G. R., Mohadesi, M., Ghanbari, M., Moradi, M. J., Hosseini, S., & Davoodbeygi, Y. (2015). Kinetic comparison of two basic heterogenous catalysts obtained from sustainable resources for transesterification of waste cooking oil. *Biofuel Research Journal*, 6, 236–241. https://www.biofueljournal.com.

Mujeli, M., Kefas, H. M., Shitu, A., & Ayuba, I. (2016). Optimization of biodiesel production from crude cotton seed oil using central composite design. *American Journal of Chemical and Biochemical Engineering*, 1(1), 8–14. https://doi.org/10.11648/j.ajcbe.20160101.12.

Nandi, S., Bhattacharyya, R., & Ghosh, T. K. (2019). Process optimization and kinetics of biodiesel production from renewable raw materials. *Saudi Journal of Engineering and Technology*, 4(6), 248–252. https://doi.org/10.21276/sjeat.2019.4.6.2.

Noreen, S., Sahar, I., Masood, N., Iqbal, M., Zahid, M., Nisar, J., Khan, M. I., & Nazir, A. (2021). Thermodynamic and kinetic approach of biodiesel production from waste cooking oil using nano-catalysts. *Zeitschrift Für Physikalische Chemie*, 1–16. https://doi.org/10.1515/zpc-2020-1644.

Ogbole, D. A., & Ademoh, N. A. (2021). Development of a doum palm shelling machine. *International Conference on Engineering for Sustainable World (ICESW 2020)*, 1107(012193), 1–11. https://doi.org/10.1088/1757-899X/1107/1/012193.

Oladimeji, O. I., Nwadiokwu, E. P., Odogwu, D. A., Olubusoye, B. S., & Olaleye, B. V. (2022). Optimization of biodiesel production from used cooking oil using anthill as catalyst. *European Modern Studies Journal*, 6(3), 434–443. https://journal-ems.com.

Rajalingam, A., Jani, S. P., Kumar, A. S., & Khan, M. A. (2020). Production methods of biodiesel. *Journal of Chemical and Pharmaceutical Research*, 8(3), 170–173. http://www.jocpr.com/abstract/production-methods-of-biodiesel-5199.html.

Roschat, W., Butthichak, P., Daengdet, N., Phewphong, S., Kaewpuang, T., Moonsin, P., Yoosuk, B., & Promarak, V. (2020). Kinetics study of biodiesel production at room temperature based on eggshell-derived CaO as basic heterogeneous catalyst. *Engineering and Applied Science Research (EASR)*, 47(4), 361–373. https://doi.org/10.14456/easr.2020.39.

Seth, S. A., Aji, I. S., & Tokan, A. (2018). Effects of particle size and loading on tensile and flexural properties of polypropylene reinforced doum palm shell particles composites. *American Scientific Research Journal for Engineering, Technology, and Sciences (ASRJETS)*, 44(1), 231–239. http://asrjetsjournal.org.

Sharma, U., Muralidharan, N. G., Vijayalakshmi, S., & Ranjitha, J. (2020). Process optimisation and kinetics study of biodiesel production from dairy waste scum using ZnO heterogeneous nanocatalyst. *IOP Conference Series: Materials Science and Engineering 923 [ICTAMDMES'20]*, 923(012072), 1–9. https://doi.org/10.1088/1757-899X/923/1/012072.

Suleiman, K. K., Isah, M., Abdulfatai, A. S., & Danyaro, Z. (2023). Kinetics and thermodynamics study of biodiesel production from neem oil using alumina as a catalyst. *FUDMA Journal of Sciences (FJS)*, 7(3), 65–71. https://doi.org/10.33003/fjs-2023-0703-1851.

Ulfah, M., Firdaus, Sundari, E., & Praputri, E. (2020). A comparison of palm fatty acid distillate (PFAD) esterification using sulphated alumina versus sulphuric acid catalyst. *The 5th Engineering Science & Technology International Conference-IOP Conference Series: Materials Science and Engineering*, 990(012015), 1–7. https://doi.org/10.1088/1757-899X/990/1/012015.

Zahan, K. A., & Kano, M. (2018). Biodiesel production from palm oil, its by-products, and mill effluent: A review. *Energies*, 11(2132), 1–25. https://doi.org/10.3390/en11082132.